

# Structural phase transitions and fundamental band gaps of $\text{Mg}_x\text{Zn}_{1-x}\text{O}$ alloys from first principles

I. V. Maznichenko,<sup>1</sup> A. Ernst,<sup>2,\*</sup> M. Bouhassoune,<sup>2,3</sup> J. Henk,<sup>2</sup> M. Däne,<sup>1,4</sup> M. Lüders,<sup>5</sup> P. Bruno,<sup>2,6</sup> W. Hergert,<sup>1</sup> I. Mertig,<sup>2,1</sup> Z. Szotek,<sup>5</sup> and W. M. Temmerman<sup>5</sup>

<sup>1</sup>*Martin-Luther-Universität Halle-Wittenberg, Fachbereich Physik, D-06099 Halle, Germany*

<sup>2</sup>*Max-Planck-Institut für Mikrostrukturphysik, Weinberg 2, D-06120 Halle, Germany*

<sup>3</sup>*Department Physik, Universität Paderborn, 33095 Paderborn, Germany*

<sup>4</sup>*Materials Science and Technology Division, Oak Ridge National Laboratory, Oak Ridge, TN 37831, USA*

<sup>5</sup>*Daresbury Laboratory, Daresbury, Warrington, WA4 4AD, UK*

<sup>6</sup>*European Synchrotron Radiation Facility – BP 220, F-38043 Grenoble Cedex, France*

(Dated: October 30, 2018)

The structural phase transitions and the fundamental band gaps of  $\text{Mg}_x\text{Zn}_{1-x}\text{O}$  alloys are investigated by detailed first-principles calculations in the entire range of Mg concentrations  $x$ , applying a multiple-scattering theoretical approach (Korringa-Kohn-Rostoker method). Disordered alloys are treated within the coherent potential approximation (CPA). The calculations for various crystal phases have given rise to a phase diagram in good agreement with experiments and other theoretical approaches. The phase transition from the wurtzite to the rock-salt structure is predicted at the Mg concentration of  $x = 0.33$ , which is close to the experimental value of  $0.33 - 0.40$ . The size of the fundamental band gap, typically underestimated by the local density approximation, is considerably improved by the self-interaction correction. The increase of the gap upon alloying ZnO with Mg corroborates experimental trends. Our findings are relevant for applications in optical, electrical, and in particular in magnetoelectric devices.

PACS numbers: 61.50.Ks, 81.30.Hd

## I. INTRODUCTION

In recent years, much effort has been devoted to research on ZnO, inspired mostly by its attractive properties for optoelectronic applications.<sup>1</sup> This interest arises from specific properties, e. g. a large piezoelectric coefficient, photoconductivity, and transparency in the visible and infrared wavelength regimes. The range of applications of this semiconductor can be considerably extended by alloying. Prominent dopants are Co and in particular Mg, on which we focus in this work. An increase of the Mg concentration can transform the crystal lattice from the wurtzite structure (WZ) of ZnO to the rock-salt structure (RS) of MgO. Accompanied by this structural phase transition is a substantial increase of the fundamental band gap. The latter can be tuned from 3.35 eV to 7.7 eV.<sup>1,2</sup> In view of a possible band-gap engineering,  $\text{Mg}_x\text{Zn}_{1-x}\text{O}$  alloys may also be considered as suitable insulating spacers in magnetoelectronic devices, in particular in magnetic tunnel junctions.

According to the equilibrium phase diagram,<sup>3,4</sup> the solid solution of  $\text{Mg}_x\text{Zn}_{1-x}\text{O}$  is of eutectic type at normal conditions. It is characterized by an extensive solubility of zincite in MgO (up to 33 mol%) and by a restricted solubility of MgO in ZnO (4 mol%). The solubility depends strongly on experimental conditions and can be considerably increased at high temperatures and high pressures.<sup>5,6</sup> Non-equilibrium growth processes, like pulsed laser deposition (PLD)<sup>7,8,9,10,11</sup> and molecular beam epitaxial methods<sup>12,13,14,15</sup>, allow to grow high-quality  $\text{Mg}_x\text{Zn}_{1-x}\text{O}$  thin films for a large range of concentrations  $x$ . For RS- $\text{Mg}_x\text{Zn}_{1-x}\text{O}$ , produced by PLD,

a maximum solubility has been reported for  $x = 0.5$ .<sup>9,16</sup> When increasing the Zn concentration, the RS and the WZ phases separate, and  $\text{Mg}_x\text{Zn}_{1-x}\text{O}$  exhibits a WZ structure for  $x < 0.4$ .<sup>17</sup> The solubility limit and the phase formation in  $\text{Mg}_x\text{Zn}_{1-x}\text{O}$  are strongly influenced by experimental conditions and by the substrate on which the  $\text{Mg}_x\text{Zn}_{1-x}\text{O}$  film is grown. In general, alloying of ZnO and MgO proceeds by substituting Mg atoms by Zn atoms in the cubic RS structure and *vice versa* in the hexagonal WZ structure.

The composition and the crystalline structure affect directly the electronic properties of  $\text{Mg}_x\text{Zn}_{1-x}\text{O}$ . Numerous absorption and photoluminescence spectroscopy experiments show that the fundamental band gap depends differently on the Zn concentration in the RS and WZ phases.<sup>18,19</sup> The width of the band gap increases most linearly with Mg concentration for both the RS and the WZ phase, but the slope in cubic  $\text{Mg}_x\text{Zn}_{1-x}\text{O}$  is about twice as large as in the hexagonal structure.<sup>20</sup> This experimental finding clearly indicates that  $\text{Mg}_x\text{Zn}_{1-x}\text{O}$  is a promising candidate for band-gap engineering. For instance in a magnetic tunnel junction, electrons that are transmitted from one electrode to the other have to pass the nonconducting spacer.<sup>21</sup> The transmission probability decays with spacer thickness and with the width of the spacer's fundamental band gap.<sup>22,23</sup> As a consequence, the spin-dependent conductance, i. e. the tunnel magnetoresistance, could be tuned by varying the fundamental band gap. Further, the magnetoresistance depends essentially on the properties of the ferromagnet-insulator interface, as was shown for Fe/MgO/Fe tunnel junctions.<sup>24,25</sup> Hence, detailed knowledge of its geometric

structure is necessary, and our theoretical investigation of the bulk structural phases can be regarded as one step towards that goal.

In addition to the extensive experimental work, there exist many detailed theoretical studies of both ZnO and MgO. Among them are Refs. 26,27,28,29,30,31,32,33,34, 35,36, using a variety of *ab initio* computational methods. There are, however, not many studies of  $\text{Mg}_x\text{Zn}_{1-x}\text{O}$  alloys, possibly due to the complex interplay of their electronic and geometric structures. Recently, thermodynamical stability and ordering tendencies of the alloys have been carefully investigated using the cluster-expansion method.<sup>37</sup> Based on the parameterization of total energies for various alloy configurations, the latter allows to study accurately structural properties, including short-range order (SRO) effects.<sup>38,39</sup> It is found that the RS  $\leftrightarrow$  WZ transition occurs at  $x \approx 0.33$ , which is consistent with experiment ( $x = 0.33$ , Ref. 7; similar results were obtained by a pseudopotential method using supercells<sup>40</sup>). The cluster expansion method was also used by Seko *et al.* for investigating phase transitions, including vibrational effects through lattice dynamics calculations.<sup>41</sup> The authors demonstrate that the transition pressure decreases with increasing Mg content, which is explained as follows. Below the solubility limit of MgO in ZnO, the RS phase is energetically preferred to the WZ phase in MgO. Above the solubility limit, the configurational entropy increases by the transition from a mixed WZ-ZnO/RS-MgO to a RS single phase.

A brief critical review of previous theoretical *ab initio* investigations has shown that: (i) In ZnO, the energy levels of the localized Zn-3*d* electrons are found relatively high and thus close to the valence bands, resulting in strong hybridization with O-2*p* states. Since these hybridization effects have to be correctly taken into account, the all-electron methods are preferred to the pseudopotential methods in which localized electrons are neglected. (ii) Because the Zn-3*d* electrons are localized, they are not well described within the local spin density approximation (LSDA) to density functional theory (DFT). To treat these electronic states adequately, one has to go beyond the LSDA, for example by applying the self-interaction correction (SIC) to the LSDA. (iii) Previous studies often focused on the WZ and RS structures of the ordered alloys (i. e.  $x = 0$  or 1). A detailed investigation of the complete transition path (with continuous variation of  $x$ ) is still missing. For the latter it is inevitable to treat disordered alloys, for example within the coherent potential approximation.

In the present paper, we report on a systematic first-principles study of structural and electronic properties of ordered and disordered  $\text{Mg}_x\text{Zn}_{1-x}\text{O}$  alloys using an all-electron full-charge density Korringa-Kohn-Rostoker (KKR) method.<sup>42,43</sup> Alloying of MgO and ZnO is described within CPA,<sup>44</sup> as formulated in multiple-scattering theory (KKR-CPA).<sup>45</sup> One objective of this investigation is to describe accurately the structural phase transition from the WZ to the RS structure in

$\text{Mg}_x\text{Zn}_{1-x}\text{O}$ , by continuously increasing the Mg concentration. The second objective addresses the formation of the fundamental band gap in  $\text{Mg}_x\text{Zn}_{1-x}\text{O}$ . It is further shown how the hybridization between Zn-3*d* and O-2*p* states affects the width of the band gap, by comparing results obtained within the LSDA with those obtained by applying the self-interaction correction.<sup>46,47</sup> The validity of the present approach, especially the use of the CPA, is discussed by comparing our results with those of previous studies.<sup>37,40,41</sup> In summary, our study addresses important issues in  $\text{Mg}_x\text{Zn}_{1-x}\text{O}$  alloys which, with respect to magnetic tunnel junctions, might also be relevant for magnetoelectronics.

The paper is organized as follows. The model of the transition path from the WZ to the RS structure is sketched in Section II. Details of the computational approach are presented in Section III. Results are discussed in Section IV. By comparing our results for the ordered alloys with those of other theoretical work and with experiment, the validity of our approach has been established. Our main results for the disordered alloys are discussed in Section V. In Section VI, the formation and evolution of the fundamental band gap as a function of Mg and Zn contents in the system is analyzed. Concluding remarks close the paper in Section VII.

## II. MODELING THE STRUCTURAL WZ $\leftrightarrow$ RS PHASE TRANSITION

To investigate structural phase transitions in  $\text{Mg}_x\text{Zn}_{1-x}\text{O}$ , a transition path suggested for the continuous structural WZ  $\leftrightarrow$  RS transformation in GaN was adopted.<sup>31</sup> This path has been already successfully applied in studies of structural deformations in MgO<sup>32</sup> and in ZnO.<sup>48</sup> The structural transition is described as a homogenous strain deformation from the WZ to the RS phase by passing an intermediate hexagonal structure (HX, referred to as *h*-MgO in Ref. 31). This hexagonal structure can as well occur in epitaxial systems due to the reduction of the interlayer distance, which was recently observed for thin ZnO films.<sup>49,50</sup> A similar scheme is the Bain's path for the transition from the face-centered-cubic to the body-centered-cubic structure.<sup>51</sup>

In the first step on the transition path (WZ  $\leftrightarrow$  HX), the internal parameter  $u$  is linearly increased while simultaneously decreasing the  $c/a$  ratio (Fig. 1). At  $u = 1/2$  the space group changes from  $P6_3mc$  to  $P6_3/mmc$ . In the second step (HX  $\leftrightarrow$  RS), the lattice is compressed uniaxially along the  $[10\bar{1}0]$  direction and simultaneously  $c/a$  is decreased further. The WZ phase is characterized by  $a = b$ ,  $c/a = \sqrt{8/3}$ ,  $v = 1/3$  and  $u = 3/8$ , whereas the HX phase has  $a = b$ ,  $c/a = 1.2$ ,  $v = 1/3$ , and  $u = 1/2$ . For the RS phase,  $a = b = c$  and  $v = u = 1/2$ . For details, see Ref. 32.

To perform total-energy minimizations (see Section III), the appropriate unit cell of an orthorhombic

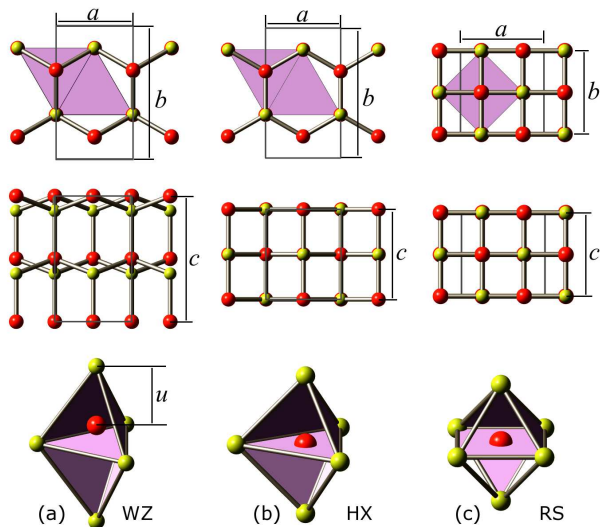


FIG. 1: (Color) Structural phases in  $\text{Mg}_x\text{Zn}_{1-x}\text{O}$ . The wurtzite structure (a: WZ, left column), the intermediate hexagonal structure (b: HX, central column), and the rock-salt structure (c: RS; right column) are shown in top view (top row) and in side view (central row). The hexahedral chemical units are depicted in the bottom row. The lattice parameters  $a$ ,  $b$ , and  $c$  for the common space group  $Cmc2_1$  are indicated. The  $xy$ -plane of unit cells for  $P6_3mc$ ,  $P6_3/mmc$ , and  $Fm\bar{3}m$  space groups for WZ, HX, and RS respectively are displayed in the top row in magenta.  $u$  describes the internal displacement of cations sites (red, dark spheres) with respect to the central planes of the polyhedra. For  $u = 1/2$ , metal sites lie within the central planes which are spanned by the oxygen sites (yellow, bright spheres).

lattice with space group  $Cmc2_1$  was used (Fig. 1). The latter is a common subgroup of all three phases.<sup>52</sup> In our calculations, the parameter  $v$ , specifying the relative positions of the sublattices,<sup>32</sup> and the ratio  $b/a$  (defined in Fig. 1) are fixed by the geometry of a particular phase. The parameter  $u$ , which is the internal vertical displacement of the cation atoms in the oxygen plane, and the  $c/a$  ratio were obtained by the total energy minimization for the pure compounds (i. e., WZ-ZnO and RS-MgO) within LSDA. They are kept fixed at these values for  $\text{Mg}_x\text{Zn}_{1-x}\text{O}$  alloys for all concentrations  $x$ .

### III. COMPUTATIONAL DETAILS

The electronic and geometric structures of  $\text{Mg}_x\text{Zn}_{1-x}\text{O}$  alloys are obtained within density-functional theory. The local density approximation and its self-interaction correction (see below) are implemented in a multiple-scattering approach (the Korringa-Kohn-Rostoker method, KKR).<sup>53</sup> Disordered alloys are described within the coherent potential approximation (CPA).<sup>54</sup>

For closed-packed systems, for example transition metals, the crystal potential is commonly approximated as a

sum over the so-called ‘muffin-tin potentials’<sup>55</sup> (that is, spherically symmetric potentials centered at each lattice site, while in the interstitial region the potential is constant). For open systems, this approximation results in a relatively poor description of the electronic structure. It has turned out that the usual trick of inserting the so-called ‘empty spheres’ into the interstitial region is not sufficient for MgO and ZnO, in particular in view of the high degree of accuracy needed in the evaluation of total energies. Obviously, the latter is inevitable for a reliable description of structural phase transitions. Consequently, a full-charge density approximation was applied. Here, the total energy is estimated from the non-spherical charge density and the full potential. All radial integrals are calculated using the unit cell geometry; the single-site problem is still solved with a spherical potential averaged within a Voronoi cell. The accuracy of this approach is as good as that of a full-potential method but is not as time-consuming. The validity of the full charge-density approximation was checked by comparison with results of the corresponding KKR full-potential calculations for the ordered WZ-ZnO and RS-MgO compounds.

The disordered  $\text{Mg}_x\text{Zn}_{1-x}\text{O}$  can be viewed as a substitutional binary alloy in which the metal sublattice (Zn, Mg) is subject to chemical disorder. The oxygen sublattice remains unaffected. Hence, the coherent potential approximation (CPA) is an obvious choice for describing  $\text{Mg}_x\text{Zn}_{1-x}\text{O}$  at an arbitrary concentration  $x$ . Within the CPA, Mg and Zn impurities are embedded into an effective coherent potential medium which is determined self-consistently.<sup>53,54</sup> Since the KKR-CPA is a single-site approximation, it does not allow to investigate the influence of chemical short-range order on the electronic properties (SRO can be taken into account by the cluster CPA,<sup>56</sup> the locally self-consistent Green function method<sup>57</sup> or the non-local CPA approach<sup>58</sup>). However, for many alloys the single-site CPA provides a reasonable description of the electronic structure.<sup>59</sup> For  $\text{Mg}_x\text{Zn}_{1-x}\text{O}$ , the validity of the KKR-CPA was established through a direct comparison with KKR supercell calculations (which include SRO effects) for  $x = 0.25, 0.50$ , and  $0.75$ . The major structural and electronic properties, such as the equilibrium lattice constants, bulk moduli, equilibrium pressures, and fundamental band gaps, are reproducible within both the KKR-CPA and the supercell approach. Hence we conclude that SRO effects cannot be ruled out but they are of minor importance for the issues addressed in this work. A detailed investigation of SRO effects is beyond the scope of the present work.

Although the Mg-2p electron states lie comparably deeply in energy (about 2 Rydberg below the valence bands), they have been treated as valence states. It is found that the hybridization of the associated electronic states with the valence states is important for an accurate determination of total energies, especially for the evaluation of both the  $c/a$  ratio and the parameter  $u$  in the WZ structure. The same procedure was applied in an earlier all-electron study of MgO, using a full-potential

linearized muffin-tin orbital (FP-LMTO) method.<sup>32</sup>

Since the Zn-3*d* states are energetically close to the O-2*p* states, they have to be considered as valence electrons as well. It is well-known that the hybridization of the localized Zn-3*d* electrons with the O-2*p* electrons is crucial for an accurate investigation of the band-gap formation in ZnO.<sup>60</sup> Being strongly localized, the Zn-3*d* states are not adequately described within the local density approximation. The LSDA contains the (unphysical) self-interaction of an electron with itself (see e. g. Refs. 47 and 61), an effect whose importance increases with the degree of electron localization. As a consequence of the self-interaction, the energy levels of the localized electrons obtained within the LSDA lie too high and their hybridization with the O-2*p* states is too strong. The calculated fundamental band gap in ZnO is therefore considerably too small as compared to experiment.

An improved description of localized electrons is achieved by the self-interaction correction<sup>46,47</sup> in which the unphysical self-interaction is removed from the LSDA exchange-correlation functional. In this approach, SIC is applied to various configurations of localized electron states, and the configuration with the lowest total energy defines the ground state energy and configuration. The SIC-LSD approach, being based on a variational principle, is parameter free and treats on equal footing both itinerant and localized electrons. When no localized electrons are present in the system, then the SIC-LSDA total energy is equivalent to the LSDA total energy. Thus the LSDA energy functional is a local minimum of the SIC-LSDA functional. For ZnO in both the RS and the WZ phase it is found that all 3*d*-electrons have to be SI-corrected. Since the Zn-3*d* states have semi-core character, application of the SIC leads to a uniform increase of the binding energies of these states, to a decrease of the total energy, and to an increased fundamental band gap in ZnO. Because other electronic states were treated within the LSDA, we label this calculations SIC-LSDA for short.

To check whether SIC affects only the fundamental band gap or also structural properties, we have compared results of a SIC-LSDA calculation for ZnO with those of an LSDA calculation, based on the same computer code. It has been shown that structural properties calculated within both LSDA and SIC-LSDA are very close, whereas the band gap obtained within SIC-LSDA has been substantially larger than in the LSDA case. This finding has been further verified for disordered Mg<sub>*x*</sub>Zn<sub>1-*x*</sub>O alloys at selected concentrations. As a result, in order to save computational costs, only LSDA has been used for the studies of the structural properties. In contrast, here, the fundamental band gap has been investigated at the respective equilibrium lattice constants within SIC-LSDA. For both the LSDA and SIC-LSDA calculations the Perdew-Wang exchange-correlation functional has been applied.<sup>62</sup>

The equilibrium volumes, bulk moduli, pressures, and enthalpies have been calculated for zero temperature from the total energy fitted to the Murnaghan equa-

tion of state.<sup>63</sup> Lattice vibrations, finite-temperature effects, and relativistic corrections have not been considered. The angular momentum cut-offs  $l_{\max}$  have been chosen as 3 for the Green function expansion and 6 for both the charge-density and the potential representation. The convergence with  $l_{\max}$  and with normalization of the Green function was significantly improved by use of Lloyd's formula in this work.<sup>64,65</sup> The concentration,  $x$ , of Mg impurities in ZnO has been varied in steps of 5%.

#### IV. STRUCTURAL PROPERTIES OF ORDERED ZnO AND MgO IN RS AND WZ PHASES

Due to the large number of structural parameters, a complete structure optimization of Mg<sub>*x*</sub>Zn<sub>1-*x*</sub>O alloys is an involved task. Apart from these parameters, the alloy composition  $x$  is an additional degree of freedom which complicates the problem further. Therefore, the number of parameters to be optimized has been reduced by concentrating on volume changes in the WZ, HX, and RS structures upon variation of  $x$  (see Section II).

To our knowledge, the KKR method was not used before for optimizing WZ and HX structures. Hence extensive calculations for pure ZnO and MgO have been required to determine both the optimum  $u$  and  $c/a$ . In accomplishing this, the procedure suggested in Ref. 32 has been followed. Since the calculation of lattice relaxations from forces is rather complicated and not sufficiently accurate within the KKR method, we have calculated the total energies consecutively varying three parameters: the lattice constants  $a$ , the  $c/a$  and the internal parameter  $u$ . The total energy has been calculated at a given  $u$  for a sufficiently dense mesh of lattice constants and then fitted to the Murnaghan equation of state. The initial value of the parameter  $u$  has been taken from the experiment for a particular structure and then successively varied as long as the absolute total energy minimum has not been reached. To establish the validity of the present KKR approach for structure optimization, our results have been compared with those of other first-principles calculations. We note that our calculations for both ZnO and MgO in various structures have been carried out for the same unit cell on the same level of approximation.

The adequacy of the present approach is evidenced by the agreement with experimental data and the results of other theoretical approaches (see Tables I and II). It is found that our results agree with those obtained by the other all-electron methods, as opposed to the pseudo-potential methods. In particular, the parameters obtained in this work compare well with those reported by Limpijumnon and coworkers.<sup>32,48</sup> This agreement might be attributed to the fact that both studies follow the same optimization scheme (as suggested in Refs. 32 and 48) and that the Zn-3*d* as well as the Mg-2*p* electrons have been treated as valence electrons.

TABLE I: Properties of ZnO in the wurtzite (WZ), the hexagonal (HX), and the rock-salt (RS) phase. Equilibrium volumes  $V_0$ ,  $c/a$  ratios, internal parameters  $u$ , and bulk moduli  $B_0$  are compiled for theoretical (present work displayed in bold) and for experimental works. PPW, LCAO, and FP-LMTO are short for pseudo-potential plane waves, linear combination of atomic orbitals, and full-potential linearized muffin-tin orbital, respectively.

Phase		Theory	Experiment
WZ	$V_0$ ( $\text{\AA}^3$ )	22.80 <sup>a</sup> , <b>22.83</b> , 22.87 <sup>b</sup> , 22.91 <sup>c</sup> , 22.93 <sup>d</sup> , 23.4 <sup>ef</sup> , 23.62 <sup>g</sup> , 23.78 <sup>e</sup>	23.80 <sup>hi</sup>
	$c/a$	1.590 <sup>g</sup> , <b>1.602</b> , 1.605 <sup>e</sup> , 1.607 <sup>c</sup> , 1.608 <sup>f</sup> , 1.610 <sup>a</sup> , 1.614 <sup>b</sup> , 1.617 <sup>d</sup>	1.602 <sup>hi</sup>
	$u$	0.379 <sup>b</sup> , 0.380 <sup>agf</sup> , <b>0.381</b> <sup>c</sup>	0.382 <sup>hi</sup>
	$B_0$ (GPa)	<b>154</b> , 154 <sup>e</sup> , 155 <sup>c</sup> , 157 <sup>f</sup> , 160 <sup>g</sup> , 162 <sup>abd</sup>	143 <sup>b</sup> , 183 <sup>i</sup>
HX	$V_0$ ( $\text{\AA}^3$ )	<b>22.12</b>	
	$c/a$	<b>1.200</b>	
	$B_0$ (GPa)	<b>165</b>	
RS	$V_0$ ( $\text{\AA}^3$ )	18.70 <sup>a</sup> , 18.76 <sup>c</sup> , 18.87 <sup>d</sup> , <b>18.88</b> , 18.98 <sup>b</sup> , 19.08 <sup>g</sup> , 19.45 <sup>e</sup>	19.48 <sup>i</sup> , 19.60 <sup>h</sup>
	$B_0$ (GPa)	200 <sup>e</sup> , <b>201</b> , 203 <sup>c</sup> , 206 <sup>b</sup> , 210 <sup>a</sup> , 211 <sup>d</sup> , 219 <sup>g</sup>	202 <sup>i</sup> , 228 <sup>h</sup>

<sup>a</sup>Ref. 48: PPW.

<sup>b</sup>Ref. 30: LCAO.

<sup>c</sup>Ref. 36: LCAO.

<sup>d</sup>Ref. 41: PPW.

<sup>e</sup>Ref. 40: PPW.

<sup>f</sup>Ref. 66: FP-LMTO.

<sup>g</sup>Ref. 67: FP-LMTO.

<sup>h</sup>Ref. 27.

<sup>i</sup>Ref. 68.

TABLE II: As Table I, but for MgO. Missing references are given in Table I.

Phase		Theory	Experiment
WZ	$V_0$ ( $\text{\AA}^3$ )	22.50 <sup>j</sup> , 22.53 <sup>e</sup> , 23.15 <sup>f</sup> , <b>23.20</b>	
	$c/a$	1.550 <sup>e</sup> , <b>1.610</b> , 1.620 <sup>j</sup> , 1.633 <sup>f</sup>	
	$u$	<b>0.380</b> , 0.380 <sup>j</sup>	
	$B_0$ (GPa)	<b>121</b> , 131 <sup>e</sup> , 137 <sup>j</sup>	
HX	$V_0$ ( $\text{\AA}^3$ )	20.90 <sup>j</sup> , <b>21.71</b>	
	$c/a$	<b>1.200</b> , 1.200 <sup>j</sup>	
	$B_0$ (GPa)	<b>135</b> , 148 <sup>j</sup>	
RS	$V_0$ ( $\text{\AA}^3$ )	17.54 <sup>e</sup> , 17.80 <sup>j</sup> , 17.96 <sup>d</sup> , 18.03 <sup>b</sup> , <b>18.19</b> , 18.65 <sup>k</sup>	18.67 <sup>l</sup> , 18.75 <sup>m</sup>
	$B_0$ (GPa)	<b>167</b> , 170 <sup>e</sup> , 172 <sup>k</sup> , 174 <sup>d</sup> , 178 <sup>j</sup> , 186 <sup>b</sup>	169 <sup>n</sup> , 172 <sup>o</sup>

<sup>j</sup>Ref. 32: FP-LMTO.

<sup>k</sup>Ref. 33: FP-KKR.

<sup>l</sup>Ref. 69.

<sup>m</sup>Ref. 70.

<sup>n</sup>Ref. 71.

<sup>o</sup>Ref. 72.

As for the structural properties, we find agreement concerning the volume ratios of the different phases and the equilibrium pressures at the phase transitions (see Tables III and IV). For ZnO there is only the WZ  $\leftrightarrow$  RS phase transition while for MgO there are two transitions, namely RS  $\leftrightarrow$  HX and RS  $\leftrightarrow$  WZ. In particular for ZnO, our theoretical results compare well with experimental ones (see Table III). For MgO we find agreement with other theoretical estimations too (Table IV). However, the equilibrium pressure for the RS-HX phase transition might be an exception. The apparent disagreement with the result reported in Ref. 32 may be related to the instabilities of the WZ and the HX structures (Figs. 2 and 3a). Moreover, due to the negative pressure these phases cannot be realized experimentally, hence ruling out a clar-

TABLE III: Structural phase transition in ZnO. Given are the volume ratio and the equilibrium pressure at the WZ  $\leftrightarrow$  RS phase transition. References as in Table I. Present work displayed in bold.

	Theory	Experiment
$V_{\text{WZ}}/V_{\text{RS}}$	1.20 <sup>b</sup> , <b>1.21</b> , 1.22 <sup>cde</sup> , 1.24 <sup>g</sup>	1.21 <sup>i</sup> , 1.22 <sup>h</sup>
$P_{\text{WZ} \leftrightarrow \text{RS}}$ (GPa)	3.9 <sup>c</sup> , 6.6 <sup>c</sup> , 8.0 <sup>g</sup> , 8.2 <sup>a</sup> , <b>8.6</b> , 8.7 <sup>c</sup>	8.7 <sup>h</sup> , 9.1 <sup>i</sup>

ifying comparison of theory with experiment. In favor of our work, we would like to mention that the present calculations reproduce well  $c/a$  and  $u$ . One might speculate that earlier implementations of multiple-scattering theory failed to optimize these structural parameters in

TABLE IV: As Table III, but for MgO. For MgO there are two transitions, RS  $\leftrightarrow$  HX and RS  $\leftrightarrow$  WZ. Experimental data are not available. References as in Table II. Present work displayed in bold.

	Theory
$V_{\text{HX}}/V_{\text{RS}}$	$1.17^j$ , <b>1.19</b>
$P_{\text{RS}\leftrightarrow\text{HX}}$ (GPa)	$-16.2^j$ , <b>-8.5</b>
$V_{\text{WZ}}/V_{\text{RS}}$	<b>1.24</b> , $1.26^j$ , $1.28^e$
$P_{\text{RS}\leftrightarrow\text{WZ}}$ (GPa)	<b>-11.1</b> , $-8.4^j$

any open structure due to the slow angular momentum convergence of the Green function (see Section III; the convergence is significantly improved by using Lloyd's formula).<sup>73</sup>

In summary, the agreement of our results for the ordered alloys with those of other theoretical investigations and experiments indicates that the present approach is as reliable and accurate as any other state-of-the-art methods.

## V. STRUCTURAL PROPERTIES OF DISORDERED $\text{Mg}_x\text{Zn}_{1-x}\text{O}$ ALLOYS

Having established that our results for ordered ZnO and MgO are consistent with the structural properties obtained by other theoretical methods and by experiments, we now turn to the discussion of results for disordered  $\text{Mg}_x\text{Zn}_{1-x}\text{O}$  alloys. To reduce the number of parameters to be optimized, both  $c/a$  and  $u$  were fixed respectively to 1.6 and 0.38 in the WZ structure and to 1.2 and 0.5 in the HX structure. This approximation is justified by the weak dependence of both  $c/a$  and  $u$  on the atomic species (Mg or Zn; cf. Tables I and II). Consequently, the structure (the actual phase), Mg concentration  $x$ , and unit cell volume remain to be varied. The results of the total-energy calculations involving these three variables are discussed below. The results of the total energy calculations are comprised in the formation enthalpy (at  $T=0$ )

$$\Delta H_\alpha(\text{Mg}_x\text{Zn}_{1-x}\text{O}) = E_\alpha(\text{Mg}_x\text{Zn}_{1-x}\text{O}) - xE_{\text{RS}}(\text{MgO}) - (1-x)E_{\text{WZ}}(\text{ZnO}) \quad (1)$$

of a structure  $\alpha$  of  $\text{Mg}_x\text{Zn}_{1-x}\text{O}$ , relative to the most stable forms of ZnO (WZ) and MgO (RS) compounds.<sup>37</sup>

The formation enthalpy is positive throughout, as seen in Fig. 2, in agreement with previous theoretical studies.<sup>37,41</sup> There are two global minima (i.e. the most stable phases; black, dark regions), for pure ZnO in WZ ( $x=0$ ) and pure MgO in RS phase ( $x=1$ ). This finding implies a tendency towards phase separation if the integration of different constituents into the medium cannot be maintained.<sup>37</sup>

In the following, five special cases are discussed in more detail, namely  $x=0.0$ , 0.33, 0.52, 0.71, and 1.0.

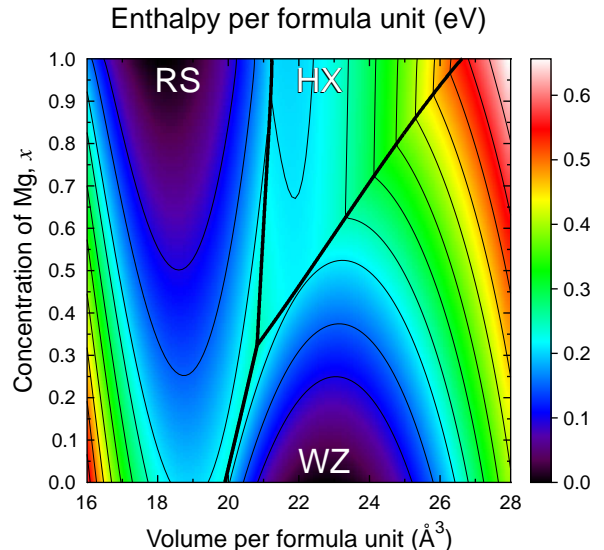


FIG. 2: (Color) Formation enthalpy of  $\text{Mg}_x\text{Zn}_{1-x}\text{O}$  alloys versus equilibrium volume and Zn concentration, depicted as color scale [cf. eq. (1)]. Straight bold lines mark separations between the phases (WZ, HX, and RS).

With low Mg concentration, the WZ phase is favorable in any case (Fig. 3a). The pressure needed for a WZ  $\leftrightarrow$  RS transition is positive and increases monotonously (Fig. 4).

For  $x < 0.33$  the total energy of the HX structure is larger than for the RS and the WZ phases, implying that an intermediate HX phase cannot be established (Fig. 2). Consequently, a direct WZ  $\leftrightarrow$  RS transition is possible at positive pressure. At  $x = 0.33$  (Figs. 3b and 5) this phase transition can take place at zero pressure. This finding is consistent with the theoretical work of Sanati and coworkers<sup>37</sup> and is also observed experimentally in ZnO-MgO heterostructures.<sup>7</sup>

At  $x = 0.71$  the WZ  $\leftrightarrow$  HX and the HX  $\leftrightarrow$  RS transitions occur at the same pressure (Fig. 4). This is evident from Fig. 3c because all total energy curves can be connected by a single tangent. We note that for  $x = 0.52$  the WZ  $\leftrightarrow$  HX transition is possible at zero pressure, and the corresponding total energies relative to RS phase are identical (see Fig. 5).

For pure MgO ( $x=1.0$ ; Fig. 3d), the RS structure exhibits the global minimum at a volume of  $18.19 \text{ \AA}^3$  which is about 2% less than the experimental value (see Table II). By applying a negative pressure (i.e. by increasing the volume along the tangent) the RS phase is transformed into the HX structure, in agreement with the work of Limpijumnong and coworkers.<sup>32</sup>

According to the phase diagram (Fig. 2), the HX phase is an intermediate phase between the WZ and RS structure for  $0.33 \leq x \leq 1.00$ . Although the HX  $\leftrightarrow$  RS transition pressure increases with Mg content, it remains neg-

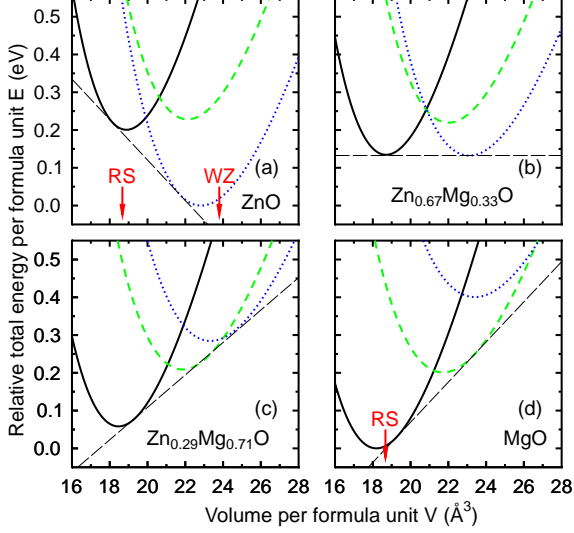


FIG. 3: (Color online) Relative total energies of  $\text{Mg}_x\text{Zn}_{1-x}\text{O}$  alloys in RS (black solid line), HX (green dashed line), and WZ (blue dotted line) structures at four different concentrations: (a)  $x = 0.0$  (pure ZnO), (b)  $x = 0.33$ , (c)  $x = 0.71$ , and (d)  $x = 1.0$  (pure MgO). Total energies in cases (a) are taken relative to the WZ phase at  $x = 0.0$  and, in (b), (c), and (d), relative to the Mg phase at  $x = 1.0$ . Red arrows show experimental values of volume (see Tables I and II)

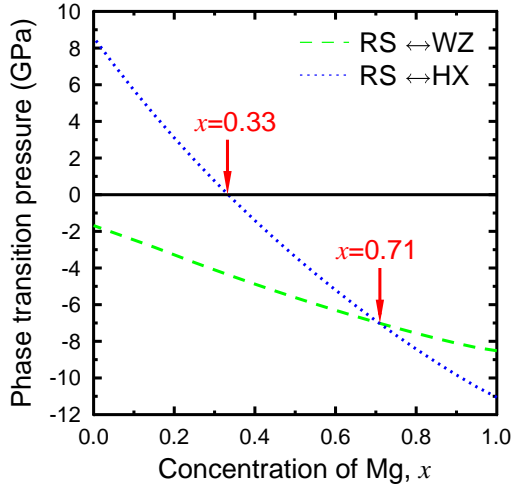


FIG. 4: (Color online) Equilibrium pressure in  $\text{Mg}_x\text{Zn}_{1-x}\text{O}$  alloys: RS  $\leftrightarrow$  WZ (green dashed line) and RS  $\leftrightarrow$  HX (blue dotted line).

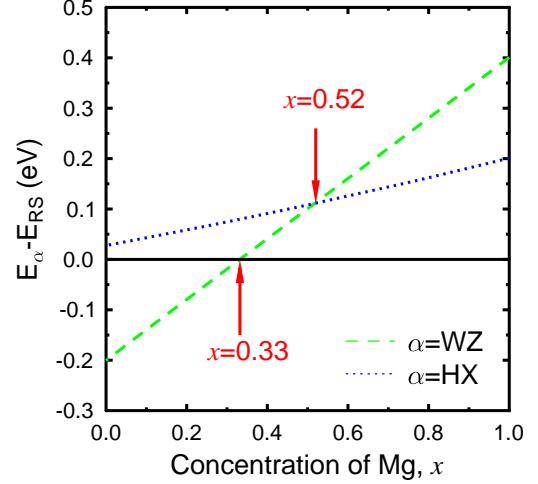


FIG. 5: (Color online) Total energies of  $\text{Mg}_x\text{Zn}_{1-x}\text{O}$  alloys in the HX (blue dashed line) and the WZ (green dotted line) structures, taken relative to the total energy of the RS structure at equilibrium volumes.

ative in the whole range of concentrations (Fig. 4).

## VI. BAND GAP IN $\text{Mg}_x\text{Zn}_{1-x}\text{O}$ ALLOYS

Since  $\text{Mg}_x\text{Zn}_{1-x}\text{O}$  alloys arouse great interest as band gap-engineering materials, in this section we study the evolution of their fundamental band gap as a function of the Zn and Mg contents. We restrict our consideration to the RS and WZ phases, as only these appear interesting from the experimental point of view.

Band gap formation can be correctly described only within a many-body theory which takes properly into account the electron-hole excitations. However, the *GW* approximation<sup>74</sup>, probably the most popular first-principles many-body approach for calculating excitation energies, is too expensive for studying alloys with arbitrary concentrations and also having constituents with localized electrons. Therefore, for this study we have used only the LSDA and SIC-LSDA approaches. The calculated band gaps have been estimated from the density of states (DOS), band structure and Bloch spectral function, corresponding to the theoretical equilibrium lattice structure of a given chemical composition.

Using LSDA for RS-MgO we obtain a band gap of 5.15 eV, which is 67% of the experimental value (7.7 eV). For the pure WZ-ZnO, LSDA gives the band gap of 0.8 eV, which is only 23% of the experimental value of 3.35 eV. In MgO, the difference between the calculated and experimental values originates mostly from the fact that the electron-hole excitations are neglected in

LSDA, which can be corrected effectively with the *GW* approximation.<sup>75</sup> For ZnO the problem is more complex, as in addition to the neglect of the electron-hole excitations, the localized nature of Zn 3*d* electrons is not adequately represented within LSDA. This failure of LSDA is largely related to the inherent unphysical self-interaction. The latter affects the band gap by placing the localized 3*d* electrons of Zn at too low binding energies, thus leading to their strong hybridization with the O-2*p* states. In LSDA the Zn-3*d* states are about 3 eV too high with respect to the experimental value of about 7.5 eV–8.5 eV<sup>76,77</sup> (see the DOS of ZnO in Fig. 6). In the RS and WZ phases, the 3*d* states are placed at slightly different energies, and in the RS the corresponding band width is larger due to the more closed-packed crystal environment. The strong *pd*-hybridization dramatically reduces the band gap, which can be improved only slightly within the *GW* approximation, if based on the LSDA Green's function.<sup>60</sup> It is the aim of our future studies to use the SIC-LSDA band structure of ZnO for the subsequent *GW* calculation. The SIC-LSDA band gap we have calculated is 2.42 eV for WZ-ZnO and 2.96 eV for RS-ZnO. Thus, the SIC-LSDA band gap for the WZ-ZnO constitutes 69% of the experimental value of 3.35 eV. This tells us that SIC-LSDA is at least as good for the pure ZnO, as LSDA is for the pure MgO. The reason being, that SIC-LSDA describes both itinerant and localized electrons on equal footing. Of course, in MgO the band gap is constituted by the *sp* electrons which are itinerant and thus unaffected by the spurious self-interaction, while in ZnO the 3*d* electrons of Zn play a defining role in establishing the band gap. The SIC-LSDA approach, by removing the unphysical self-interaction of all 10 Zn *d* electrons, describes them much more adequately than LSDA. What happens as a result of SIC is that all the *d*-states of Zn move to higher binding energies and the Zn-derived bands become narrower thereby reducing the *pd*-hybridization and increasing the band gap, as seen in Fig. 6. The structural properties of  $\text{Mg}_x\text{Zn}_{1-x}\text{O}$  are believed to be little affected by this uniform shift downwards in energy of the *d*-states, leading mostly to a uniform lowering of the total energy.

Being an effective one-electron ground state theory, SIC-LSDA does not provide a quasi-particle spectrum to compare with spectroscopies. Missing the crucial screening/relaxation effects (self-energy), it predicts the 3*d* Zn electrons at too high binding energies, as opposed to LSDA where they come out too low (Fig. 6). One can implement a simple fix to correct for the screening effects in SIC-LSDA, based on the Slater's transition state theory.<sup>78,79</sup> Following the concept of the latter, we calculate the SIC-LSDA-based removal energies of localized electrons as an average of the calculated SIC-LSDA and LSDA *d*-state expectation values

$$\varepsilon_{TSA} = \frac{1}{2}(\langle d|H_{LSDA} + V_{SIC}|d\rangle + \langle d|H_{LSDA}|d\rangle). \quad (2)$$

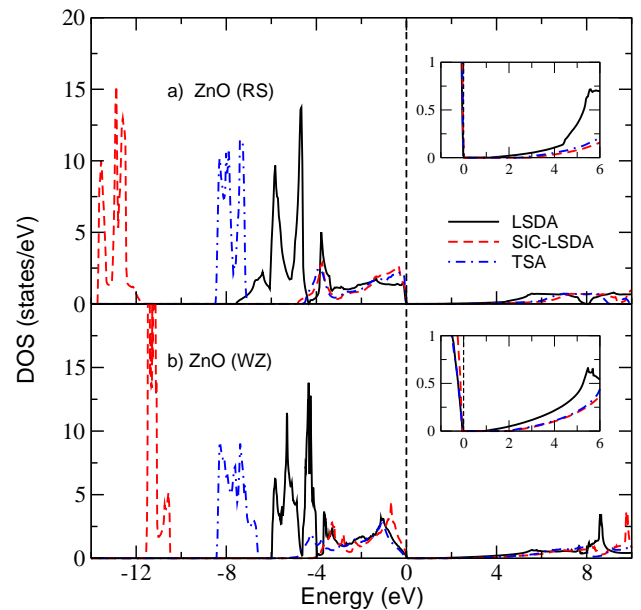


FIG. 6: (Color) Density of states (DOS) of ZnO in the RS (a) and the WZ (b) phase obtained with the LSDA (black solid lines), the SIC-LSDA (red dashed lines) and SIC-TSA (blue dash-dotted lines) approaches. Insets show the behaviour of

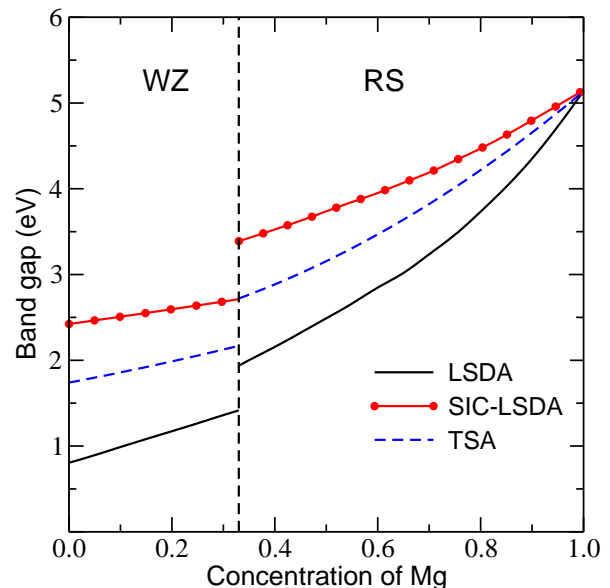


FIG. 7: (Color online) Band gaps of  $\text{Mg}_x\text{Zn}_{1-x}\text{O}$  alloys in the RS and WZ phases versus Mg content, calculated within LSDA and SIC-LSDA (line styles as indicated).

Effectively, the above equation states that only half of the SIC potential should be applied at the stage of calculating the density of states, after the self-consistency has been achieved. We refer to Eq. 2 as the transition state approximation (TSA) and show the resulting DOS of ZnO in Fig. 6. We can see that Zn *d*-states, calculated



TABLE V: The band gap  $E_g$  for MgO (RS), ZnO(WZ) and the bowing parameter for  $\text{Mg}_x\text{Zn}_{1-x}\text{O}$  alloys.

	LSDA	TSA	SIC-LSDA	Experiment
Band gap [eV]				
RS-MgO	5.15			7.70
WZ-ZnO	0.80	1.74	2.42	3.35
Bowing parameter [eV]				
RS	1.90	0.91	0.59	$0.70 \pm 0.2^{18}$
WZ	4.88	4.05	3.65	$3.60 \pm 0.6^{19}$

using TSA, appear at lower binding energies, as compared to the strict SIC-LSDA result. Consequently, the TSA-binding energies of Zn  $d$  states are in better agreement with experimental values of 7.5 eV–8.5 eV<sup>76,77</sup>. The effective hybridization of Zn  $d$ -states with the oxygen  $p$ -states is stronger as in the SIC-LSDA case, which leads to a reduction of the band gap to 2.32 eV and 1.74 eV (52% of the experimental value) in RS and WZ phases, respectively.

In  $\text{Mg}_x\text{Zn}_{1-x}\text{O}$  alloys the size of the band gap depends on the concentration of Mg impurities, as seen in Fig. 7 and Table V. While at the Mg rich end the LSDA band gaps are closer to experiment, at the other end the SIC-LSDA band gaps are more adequate. As for the TSA results, they fall mostly in between the LSDA and SIC-LSDA band gaps, especially for small Mg concentrations, where the hybridization of the O  $2p$  bands with the Zn  $3d$  states is of great significance (see Fig. 7). The behaviour of the band gap as a function of Mg concentration is also different between the various approaches. While the LSDA curves are rather parabolic, the SIC-LSDA and TSA band gaps seem to change almost linearly with concentration, thus following more closely experimental results<sup>18,19</sup>. This is mostly due to the fact that the actual magnitudes of the band gaps change slower with concentration in SIC-LSDA and TSA than in LSDA. The reason being that the larger Zn content, the more inadequate LSDA is and the smaller the resulting band gaps.

Although, both LSDA and SIC-LSDA underestimate the size of the band gap,  $E_g$ , its dependence on the Mg concentration,  $x$ , can be compared with experimental results. One way of doing it is to estimate the so-called bowing parameter,  $b$ , appearing in the commonly used definition of the fundamental band gap dependence on the composition  $x$ , namely

$$E_g(x) = xE_g(\text{MgO}) + (1-x)E_g(\text{ZnO}) - bx(1-x),$$

where the bowing parameter is given by

$$b = 2E_g(\text{MgO}) + 2E_g(\text{ZnO}) - 4E_g(\text{Zn}_{0.50}\text{Mg}_{0.50}\text{O}). \quad (3)$$

Thus to evaluate the bowing parameter one needs to know the band gaps of the pure MgO(RS) and ZnO(WZ), as well as their alloy with the concentration  $x = 0.5$ .

According to our total energy calculations the  $\text{Mg}_x\text{Zn}_{1-x}\text{O}$  at  $x = 0.5$  occurs in the RS phase which

is in agreement with the experiment of Chen *et al.*<sup>18</sup> However, the crystal structure of  $\text{Mg}_x\text{Zn}_{1-x}\text{O}$  thin film alloys depends strongly on the growth method. In variance to Ref. 18, the  $\text{Mg}_x\text{Zn}_{1-x}\text{O}$  films with  $x \leq 0.53$ , prepared with the PLD procedure, were found to have the WZ structure. Therefore, for direct comparison with the experiments we have used  $\text{Mg}_{0.50}\text{Zn}_{0.50}\text{O}$  in both RS and WZ phases. The resulting calculated bowing parameters for  $\text{Mg}_x\text{Zn}_{1-x}\text{O}$  alloys are presented in Table V. We can see that the LSDA systematically overestimates the bowing parameter for both structures, while the straight SIC-LSDA agrees very well with experiments. The TSA results fall in between the LSDA and SIC-LSDA values.

Summarizing this section, we have to say that despite rather good agreement of our SIC-LSD bowing parameter with experiments, to be truly predictive, one would need a more robust method like a combination of SIC and *GW*. This way we could also predict the correct magnitudes of the band gaps and enter the serious business of band gap engineering.

## VII. CONCLUSIONS AND OUTLOOK

Structural phase transitions and the fundamental band gaps of  $\text{Mg}_x\text{Zn}_{1-x}\text{O}$  alloys have been investigated by detailed first-principles calculations. The multiple-scattering theoretical approach used here (Korringa-Kohn-Rostoker method) allows to treat disordered alloys within the coherent potential approximation, that is  $\text{Mg}_x\text{Zn}_{1-x}\text{O}$  alloys with arbitrary Zn concentration  $x$ , with an accuracy as good as in other first-principles methods. The importance of treating localized states of ZnO appropriately within the framework of the local-density approximation to density-functional theory is established, thereby confirming the usefulness of the self-interaction correction.

The delicate interplay of geometry and electronic structure is not only of importance for bulk systems, as shown in this work. In nanotechnology, interfaces and surfaces play an essential role. Therefore, a correct description of disordered alloys and their electronic structure, in particular at the Fermi energy, is necessary for predicting material properties, besides confirming and explaining experimental results. However, to be fully predictive regarding the properties of such systems as  $\text{Mg}_x\text{Zn}_{1-x}\text{O}$  alloys, of importance for device applications, one needs a first-principles approach like a combination of *GW* with SIC-LSDA.

## Acknowledgments

This work is supported by the *Sonderforschungsbereich* SFB 762, "Functionality of Oxidic Interfaces". Research at the Oak Ridge National Laboratory was sponsored by the Division of Materials Sciences and Engineering, Office of Basic Energy Sciences, US Department of

Energy, under Contract DE-AC05-00OR22725 with UT-Battelle, LLC. We gratefully acknowledge H. L. Meyerheim for many stimulating discussions. The calculations

were performed at the John von Neumann Institute in Jülich and Rechenzentrum Garching of the Max Planck Society (Germany).

- 
- \* Electronic address: aernst@mpi-halle.de
- <sup>1</sup> U. Özgür, Y. I. Alivov, C. Liu, A. Teke, M. A. Reshchikov, S. Doğan, V. Avrutin, S.-J. Cho, and H. Morkoç, *Journal of Applied Physics* **98**, 041301 (2005).
  - <sup>2</sup> N. B. Chen and C. H. Cui, *Materials Science and Engineering B* **126**, 16 (2006).
  - <sup>3</sup> E. R. Segnit and A. E. Holland, *Journal of the American Ceramic Society* **48**, 409 (1965).
  - <sup>4</sup> S. Raghavana, J. P. Hajrab, G. N. K. Iyengar, and K. P. Abraham, *Thermochimica Acta* **189**, 151 (1991).
  - <sup>5</sup> A. N. Baranov, V. L. Solozhenko, C. Chateau, G. Bocquillon, J. P. Petit, G. N. Panin, T. W. Kang, R. V. Shpanchenko, E. V. Antipov, and Y. J. Oh, *J. Phys.: Condens. Matter* **17**, 3377 (2005).
  - <sup>6</sup> V. L. Solozhenko, A. N. Baranov, and V. Z. Tukevich, *Sol. State Commun.* **138**, 534 (2006).
  - <sup>7</sup> A. Ohtomo, M. Kawasaki, T. Koida, K. Masubuchi, H. Koinuma, Y. Sakurai, Y. Yoshida, T. Yasuda, and Y. Segawa, *Appl. Phys. Lett.* **72**, 2466 (1998).
  - <sup>8</sup> A. K. Sharma, J. Narayan, J. F. Muth, C. W. Teng, C. Jin, A. Kvit, R. M. Kolbas, and O. W. Holland, *Appl. Phys. Lett.* **75**, 3327 (1999).
  - <sup>9</sup> S. Choopun, R. D. Vispute, W. Yang, R. P. Sharma, T. Venkatesan, and H. Shen, *Appl. Phys. Lett.* **80**, 1529 (2002).
  - <sup>10</sup> J. Narayan, A. K. Sharma, A. Kvit, C. Jin, J. F. Muth, and O. W. Holland, *Sol. State Commun.* **121**, 9 (2002).
  - <sup>11</sup> M. Kunisu, I. Tanaka, T. Yamamoto, S. T., and T. Mizoguchi, *J. Phys.: Condens. Matter* **16**, 3801 (2004).
  - <sup>12</sup> W. I. Park, G. C. Yi, and H. M. Jang, *Appl. Phys. Lett.* **79**, 2022 (2001).
  - <sup>13</sup> T. Takagi, H. Tanaka, S. Fujita, and S. Fujita, *Jpn. J. Appl. Phys.* **42**, L401 (2003).
  - <sup>14</sup> S. Fujita, T. Takagi, H. Tanaka, and S. Fujita, *phys. stat. sol. (b)* **241**, 599 (2004).
  - <sup>15</sup> Z. Vashaei, T. Minegishi, T. Suzuki, M. W. Cho, T. You, and A. Setiawan, *J. Appl. Phys.* **98**, 054911 (2005).
  - <sup>16</sup> P. Bhattacharya, R. R. Das, and R. S. Katiyar, *Appl. Phys. Lett.* **83**, 2010 (2003).
  - <sup>17</sup> L. A. Bendersky, I. Takeuchi, K.-S. Chang, W. Yang, S. Hullavarad, and R. D. Vispute, *J. Appl. Phys.* **98**, 083526 (2005).
  - <sup>18</sup> N. B. Chen, H. Z. Wu, D. J. Qiu, T. N. Xu, J. Chen, and W. Z. Shen, *J. Phys.: Condens. Matter* **16**, 2973 (2004).
  - <sup>19</sup> R. Schmidt-Grund, D. Fritsch, B. Schubert, M. Rheinländer, H. Schmidt, H. Hochmut, M. Lorenz, D. Spemann, C. M. Herzinger, and M. Grundmann, *AIP Conf. Proc.* **772**, 201 (2005).
  - <sup>20</sup> J. Chen, W. Z. Shen, N. B. Chen, D. J. Qiu, and H. Z. Wu, *J. Phys.: Condens. Matter* **15**, L475 (2003).
  - <sup>21</sup> S. Datta, *Electronic Transport in Mesoscopic Systems* (Cambridge University Press, Cambridge, 1995).
  - <sup>22</sup> P. H. Dederichs, P. Mavropoulos, O. Wunnicke, N. Papanikolaou, V. Bellini, R. Zeller, V. Drchal, and J. Kudrnovský, *J. Magn. Magn. Mater.* **240**, 108 (2002).
  - <sup>23</sup> X.-G. Zhang and W. H. Butler, *J. Phys.: Condens. Matter* **15**, R1603 (2003).
  - <sup>24</sup> X.-G. Zhang, W. H. Butler, and A. Bandyopadhyay, *Phys. Rev. B* **68**, 092402 (2003).
  - <sup>25</sup> C. Tusche, H. L. Meyerheim, N. Jedrecy, G. Renaud, A. Ernst, J. Henk, P. Bruno, and J. Kirschner, *Phys. Rev. Lett.* **95**, 176101 (2005).
  - <sup>26</sup> J. E. Jaffe and A. C. Hess, *Phys. Rev. B* **48**, 7903 (1993).
  - <sup>27</sup> S. Desgreniers, *Phys. Rev. B* **58**, 14102 (1998).
  - <sup>28</sup> J. M. Recio, M. A. Blanco, V. Luaña, R. Pandey, L. Gerward, and J. S. Olsen, *Phys. Rev. B* **58**, 8949 (1998).
  - <sup>29</sup> N. A. Hill and U. Waghmare, *Phys. Rev. B* **62**, 8802 (2000).
  - <sup>30</sup> J. E. Jaffe, J. A. Snyder, Z. Lin, and A. V. Hess, *Phys. Rev. B* **62**, 1660 (2000).
  - <sup>31</sup> S. Limpijumng and W. R. L. Lambrecht, *Phys. Rev. Lett.* **86**, 91 (2001).
  - <sup>32</sup> S. Limpijumng and W. R. L. Lambrecht, *Phys. Rev. B* **63**, 104103 (2001).
  - <sup>33</sup> A. N. Baranov, V. S. Stepanyuk, W. Hergert, A. A. Katsnelson, A. Settels, R. Zeller, and P. H. Dederichs, *Phys. Rev. B* **66**, 155117 (2002).
  - <sup>34</sup> J. Sun, H.-T. Wang, J. He, and Y. Tain, *Phys. Rev. B* **71**, 125132 (2005).
  - <sup>35</sup> R. Laskowski and N. E. Christensen, *Phys. Rev. B* **73**, 045201 (2006).
  - <sup>36</sup> J. Uddin and G. E. Scuseria, *Phys. Rev. B* **74**, 245115 (2006).
  - <sup>37</sup> M. Sanati, G. L. W. Hart, and A. Zunger, *Phys. Rev. B* **68**, 155210 (2003).
  - <sup>38</sup> A. Zunger, in *Statics and Dynamics of Alloys Phase Transition*, edited by P. E. A. Turchi and A. Gonis (Plenum, New York, 1994), p. 361.
  - <sup>39</sup> D. B. Laks, L. G. Ferreira, S. Froyen, and A. Zunger, *Phys. Rev. B* **46**, 12587 (1992).
  - <sup>40</sup> Y.-S. Kim, E.-C. Lee, and K. J. Chang, *J. Korean Phys. Soc.* **39**, 92 (2001).
  - <sup>41</sup> A. Seko, F. Oba, A. Kuwabara, and I. Tanaka, *Phys. Rev. B* **72**, 024107 (2005).
  - <sup>42</sup> J. Koringa, *Physica* **13**, 392 (1947).
  - <sup>43</sup> W. Kohn and N. Rostoker, *Phys. Rev.* **94**, 1111 (1954).
  - <sup>44</sup> P. Soven, *Phys. Rev.* **156**, 809 (1967).
  - <sup>45</sup> B. L. Györfy, *Phys. Rev. B* **5**, 2382 (1972).
  - <sup>46</sup> J. P. Perdew and A. Zunger, *Phys. Rev. B* **23**, 5048 (1981).
  - <sup>47</sup> M. Lüders, A. Ernst, M. Däne, Z. Szotek, A. Svane, D. Ködderitzsch, W. Hergert, B. L. Györfy, and W. M. Temmerman, *Phys. Rev. B* **71**, 205109 (2005).
  - <sup>48</sup> S. Limpijumng and S. Jungthawan, *Phys. Rev. B* **70**, 054104 (2004).
  - <sup>49</sup> C. Tusche, H. L. Meyerheim, and J. Kirschner, *Phys. Rev. Lett.* **99**, 026102 (2007).
  - <sup>50</sup> H. L. Meyerheim, C. Tusche, A. Ernst, S. Ostanin, I. V. Maznichenko, K. Mohseni, N. Jedrecy, J. Zegenhagen, J. Roy, I. Mertig, et al., *Phys. Rev. Lett.* **102**, 156102 (2009).
  - <sup>51</sup> P. M. Marcus, F. Jona, and J. L. Qiu, *Phys. Rev. B* **66**, 064111 (2002).
  - <sup>52</sup> H. Sowa, *Act. Cryst.* **A57**, 176 (2001).

- <sup>53</sup> J. Zabloudil, R. Hammerling, L. Szunyogh, and P. Weinberger, eds., *Electron Scattering in Solid Matter* (Springer, Berlin, 2005).
- <sup>54</sup> A. Gonis, *Green Functions for Ordered and Disordered Systems*, vol. 4 of *Studies in Mathematical Physics* (North-Holland, Amsterdam, 1992).
- <sup>55</sup> P. Weinberger, *Electron Scattering Theory of Ordered and Disordered Matter* (Clarendon Press, Oxford, 1990).
- <sup>56</sup> P. Weinberger, R. Dirl, A. M. Boring, A. Gonis, and A. J. Freeman, Phys. Rev. B **37**, 1383 (1988).
- <sup>57</sup> I. A. Abrikosov, S. I. Simak, B. Johansson, A. V. Ruban, and H. L. Skriver, Phys. Rev. B **56**, 9319 (1997).
- <sup>58</sup> D. A. Rowlands, A. Ernst, J. B. Staunton, and B. L. Györfy, Phys. Rev. B **73**, 165122 (2006).
- <sup>59</sup> I. A. Abrikosov and B. Johansson, Phys. Rev. B **57**, 14 164 (1998).
- <sup>60</sup> M. Usuda, N. Hamada, T. Kotani, and M. van Schilf-gaarde, Phys. Rev. B **66**, 125101 (2002).
- <sup>61</sup> W. M. Temmerman, A. Svane, Z. Szotek, and H. Winter, in *Electronic Density Functional Theory: Recent Progress and New Directions*, edited by J. F. Dobson, G. Vignale, and M. P. Das (Plenum Press, New York, 1998), p. 327.
- <sup>62</sup> J. P. Perdew and Y. Wang, Phys. Rev. B **45**, 13 244 (1992).
- <sup>63</sup> F. D. Murnaghan, in Proceedings of the National Academy of Sciences **30**, 244 (1944).
- <sup>64</sup> P. Lloyd, Proc. Phys. Soc. **90**, 207 (1967).
- <sup>65</sup> R. Zeller, J. Phys.: Condens. Matt. **16**, 6453 (2004).
- <sup>66</sup> W. R. L. Lambrecht, S. Limpijumnong, and B. Segall, MRS Internet J. Nitride Semicond. Res. **4S1**, G6.8 (1999).
- <sup>67</sup> R. Ahuja, L. Fast, O. Eriksson, J. M. Wills, and B. Johansson, J. Appl. Phys. **83**, 8065 (1998).
- <sup>68</sup> H. Karzel, W. Potzel, M. Köfferlein, W. Schissl, M. Steiner, U. Hiller, G. M. Kalvius, D. W. Mitchell, T. P. Das, P. Blaha, et al., Phys. Rev. B **53**, 11425 (1996).
- <sup>69</sup> R. W. G. Wyckoff, *Crystal Structures*, vol. 1 (Interscience Publishers, New York, 1963), 2nd ed.
- <sup>70</sup> M. J. L. Sangster and A. Stoneham, Phil. Mag. B **43**, 597 (1981).
- <sup>71</sup> A. J. Cohen and R. G. Gordon, Phys. Rev. B **14**, 4593 (1981).
- <sup>72</sup> M. J. L. Sangster, G. Peckham, and D. H. Saunderson, J. Phys. C: Sol. State Phys. **3**, 1026 (1970).
- <sup>73</sup> N. Y. Maghadam, G. M. Stocks, X.-G. Zhang, D. M. C. Nicholson, W. A. Shelton, Y. Wang, and J. S. Faulkner, J. Phys.: Condens. Matt. **13**, 3073 (2001).
- <sup>74</sup> L. Hedin and S. Lundqvist, in *Solid State Physics*, edited by F. Seitz and D. Turnbull (New York: Academic, 1969), vol. 23.
- <sup>75</sup> U. Schönberger and F. Aryasetiawan, Phys. Rev. B **52**, 8788 (1995).
- <sup>76</sup> R. A. Powell, W. E. Spicer, and J. C. McMennamin, Phys. Rev. Lett. **27**, 97 (1971).
- <sup>77</sup> C. J. Vesely, R. L. Hengehold, and D. W. Langer, Phys. Rev. B **5**, 2296 (1972).
- <sup>78</sup> J. C. Slater, Advances in Quantum Chemistry **6**, 1 (1972).
- <sup>79</sup> D. A. Liberman, Phys. Rev. B **62**, 6851 (2000).